Joule

CellPress

Article

Electrosynthesis of Hydrogen Peroxide by Phase-Transfer Catalysis

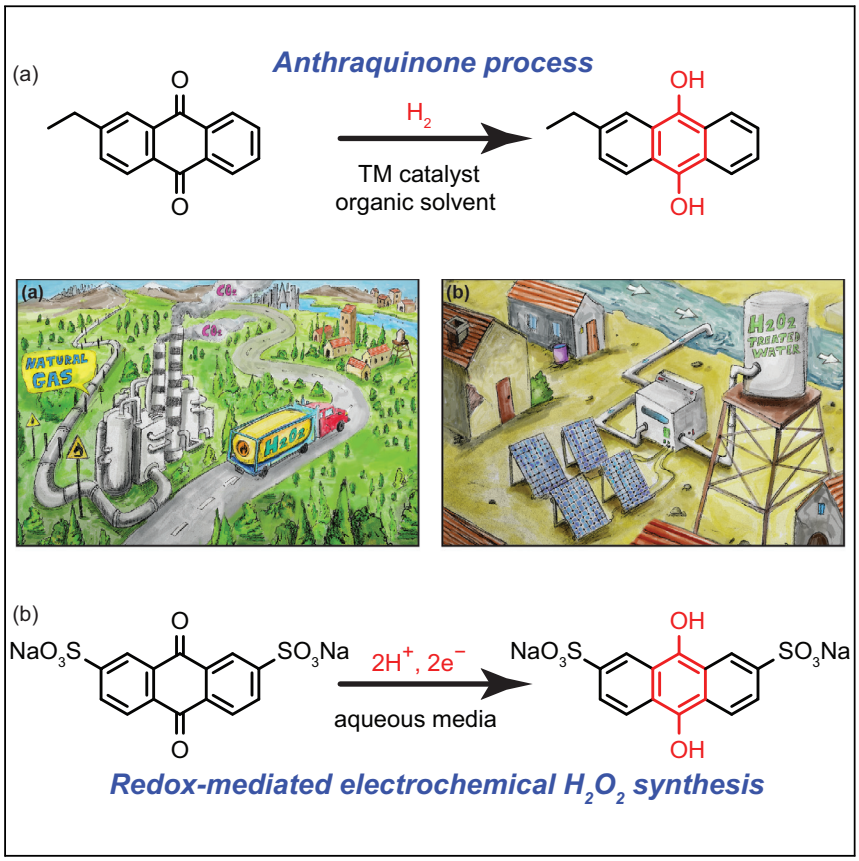

Negatively charged anthraquinones are reduced electrochemically and can generate hydrogen peroxide (H_2O_2) by partial oxygen reduction. The use of phase-transfer catalysis allows the production of the product far from the site of electrolysis, facilitating the precious metal-free synthesis of H_2O_2 in an electrolyte-free medium. A proof-of-concept device is designed to perform this process in continuous flow.

Alexander T. Murray, Sahag Voskian, Marcel Schreier, T. Alan Hatton, Yogesh Surendranath

tahatton@mit.edu (T.A.H.)
yogi@mit.edu (Y.S.)

HIGHLIGHTS

Phase-transfer catalysis shuttles redox equivalents from the site of electrolysis

Organic electrocatalysis is used to generate H_2O_2, a high-value liquid product

Hydrogen peroxide is produced in electrolyte-free media, avoiding separation steps

A flow device demonstrates long-term operation at high faradic efficiencies

Murray et al., Joule 3, 1–13
December 18, 2019
https://doi.org/10.1016/j.joule.2019.09.019

Please cite this article in press as: Murray et al., Electrosynthesis of Hydrogen Peroxide by Phase-Transfer Catalysis, Joule (2019), https://doi.org/10.1016/j.joule.2019.09.019

Joule

CellPress

Article

Electrosynthesis of Hydrogen Peroxide by Phase-Transfer Catalysis

Alexander T. Murray,[1,3,4] Sahag Voskian,[2,3] Marcel Schreier,[1] T. Alan Hatton,[2,*] and Yogesh Surendranath[1,5,*]

SUMMARY

The portable electrochemical generation of hydrogen peroxide (H_2O_2) from air and water would enable greater utilization of this versatile green oxidant in applications ranging from environmental remediation to portable sanitation. Currently, electrochemical H_2O_2 synthesis is hampered by the lack of low-cost, non-toxic catalysts that selectively reduce O_2 to H_2O_2 and the lack of low-energy methods for separating the produced H_2O_2 from the electrolyte media. Herein, we show that a disulfonated anthraquinone can simultaneously catalyze the selective conversion of O_2 to H_2O_2 and shuttle between immiscible aqueous and organic phases via ion exchange. We exploit both of these properties in a flow system to assemble an all-Earth-abundant prototype device for the continuous generation and separation of H_2O_2 into an electrolyte-free water stream. The combination of molecular redox mediation and phase-transfer catalysis demonstrated here has broad implications for the electrochemical synthesis and isolation of value-added chemicals and fuels.

INTRODUCTION

Hydrogen peroxide (H_2O_2) is a strong, environmentally benign, atom-economical oxidant that is employed in a wide variety of applications. In particular, it can be used directly at low concentrations for the disinfection of drinking water and for routine domestic sanitation needs.[1] In addition, H_2O_2 is used in advanced oxidation processes, where strongly oxidizing hydroxyl radicals (OH•), generated by the ultraviolet (UV)-light induced decomposition of H_2O_2, are employed for purification of wastewater from industrial and agricultural sources.[2,3] Indeed, a lack of access to clean water and sanitation has been linked to 2.4 million annual deaths in the developing world and contributes to childhood mortality at a rate higher than HIV, malaria, and tuberculosis combined.[4] In principle, environmental sustainability and global human health could be advanced by greater access to H_2O_2 at the point of greatest need.

The legacy method for large-scale peroxide production is the anthraquinone or Riedl-Pfleiderer process, which involves O_2 hydrogenation via a homogeneous proton/electron carrier.[5] The net reaction for this process is as follows:

$$H_2 \text{ (methane-derived)} + O_2 \rightarrow H_2O_2. \qquad \text{(Equation 1)}$$

The H_2 required for this reaction is typically sourced from steam methane reforming (SMR), a high-temperature, capital-intensive process that is challenging to downscale.[6] In 2015, close to 4.3 Mt of H_2O_2 was produced via the anthraquinone process, which consumes 17.6 kWh kg^{-1} H_2O_2, leading to an aggregate energy consumption

Context & Scale

Hydrogen peroxide (H_2O_2) is a crucial oxidant for processes as diverse as wood pulping, fine chemical synthesis, water purification, and environmental remediation. Legacy production of peroxide relies on fossil resources and is difficult to downscale. Renewable electricity can be used to drive the electrochemical synthesis of H_2O_2 directly from H_2O and O_2, but current electrochemical methods suffer from the use of precious metals, toxic catalyst materials, and the requirement of expensive downstream separation of H_2O_2 from the electrolyte. We address all of these challenges by coupling electrochemistry with phase-transfer catalysis using organic quinone mediators to furnish continuous H_2O_2 synthesis and separation.

Please cite this article in press as: Murray et al., Electrosynthesis of Hydrogen Peroxide by Phase-Transfer Catalysis, Joule (2019), https://doi.org/10.1016/j.joule.2019.09.019

of ~8.6 GWyr annually.[7] This energy is mainly supplied via fossil fuel combustion, which adds to the already substantial carbon footprint of the SMR process that precedes H_2O_2 production. The SMR process alone contributes 0.25 equiv of CO_2 per equivalent of H_2O_2, leading to a carbon footprint for H_2O_2 production of >2.8 Mt in 2015 (see Supplemental Information, p S10). Clearly, methods for driving the synthesis of H_2O_2 with renewable electricity have the potential to substantially reduce the carbon footprint associated with producing this important oxidizer.

In addition to the energy considerations described above, many applications of H_2O_2, including distributed water treatment, disinfection, and sanitation, increasingly demand portable generation of H_2O_2 at the point of use.[4–6] For these applications, an alternative to the legacy anthraquinone process is the direct synthesis of H_2O_2 from water and oxygen:

$$2\,H_2O + O_2 \rightarrow 2\,H_2O_2,\ \Delta G = +205\ kJ\ mol^{-1}\ \Delta E = -0.53\ V. \quad \text{(Equation 2)}$$

This net reaction (Equation 2) is endergonic, but can be driven electrochemically via two countervailing half-reactions; the oxidation of H_2O to O_2 (Equation 3) and the two-electron, two-proton partial reduction of O_2 to H_2O_2 (Equation 4):

$$2H_2O \rightarrow O_2 + 4H^+ + 4e^-,\ E_0 = +1.23\ V. \quad \text{(Equation 3)}$$

$$2O_2 + 4H^+ + 4e^- \rightarrow 2H_2O_2,\ E_0 = +0.70\ V. \quad \text{(Equation 4)}$$

Direct electrochemical H_2O_2 synthesis suffers from a variety of challenges. In particular, since H_2O_2 is a highly water-soluble liquid, separating the H_2O_2 product from the strongly acidic or alkaline electrolyte medium can be challenging. This separation could, in principle, be achieved via either distillation or reverse osmosis. However, distillation leads to an exorbitant energy cost for separation that is comparable to the anthraquinone process itself; reverse osmosis should have a lower input of heat (see Supplemental Information, page S10) but requires expensive membranes that may be susceptible to oxidative degradation and parasitic loss of H_2O_2 in the rejected brine.

Current electrochemical methods for H_2O_2 production can be divided into two categories. Firstly, established methods exist using carbon or modified carbon catalysts,[8–13] which often are used to produce hydroperoxide anion in strongly alkaline media. This method is generally employed for the on-site generation of the hydroperoxide anion for wood pulping applications. Alternatively, metal-based electrocatalysts can be used to generate H_2O_2 in acidic media[14–17] and have been integrated into PEM electrolysis devices, which can facilitate H_2O_2 production in electrolyte-free water.[18,19] Recently, a system has been reported using a neutralization cell whereby hydrogen peroxide is generated by recombination of HO_{2-} and H^+ through a solid electrolyte.[20] While this design generates high H_2O_2 concentrations, it also requires a precious metal anode and may be liable to H_2O_2 crossover at high current density.

Despite these advances, challenges in electrochemical H_2O_2 synthesis remain. Many H_2O_2-forming catalysts are also active for the direct reduction of O_2 to H_2O, and the parasitic disproportionation of the synthesized H_2O_2 to O_2 and H_2O, leading to low selectivity.[14,18,19,21,22] Additionally, many state-of-the-art

[1]Department of Chemistry, Massachusetts Institute of Technology, Cambridge, MA 02139, USA

[2]Department of Chemical Engineering, Massachusetts Institute of Technology, Cambridge, MA 02139, USA

[3]These authors contributed equally

[4]Present address: School of Physical Sciences, University of Kent, Canterbury, Kent CT2 7NH, UK

[5]Lead Contact

*Correspondence: tahatton@mit.edu (T.A.H.), yogi@mit.edu (Y.S.)

https://doi.org/10.1016/j.joule.2019.09.019

Please cite this article in press as: Murray et al., Electrosynthesis of Hydrogen Peroxide by Phase-Transfer Catalysis, Joule (2019), https://doi.org/10.1016/j.joule.2019.09.019

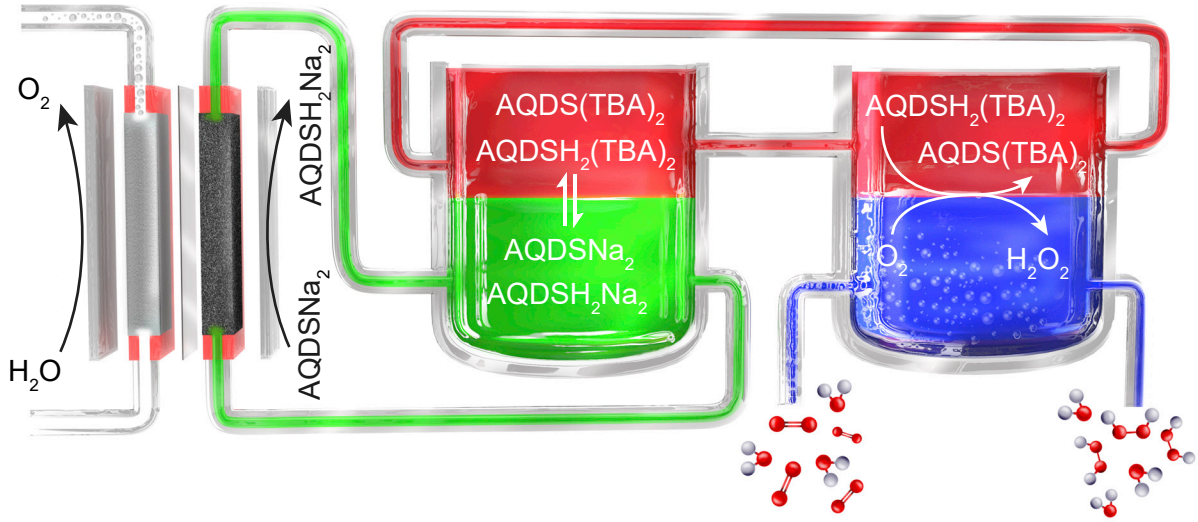

Figure 1. Schematic of Overall Phase-Transfer Approach to Electrochemical H_2O_2 Production

The scheme depicts the electrochemical cell (left) carrying out mediator reduction and water oxidation, phase-transfer of the mediator (middle) between the electrolyte (green) and organic (red) phase, and H_2O_2 production and extraction (right) from the organic phase to generate a pure aqueous H_2O_2 stream (blue).

electrocatalysts for direct H_2O_2 synthesis employ precious metals with toxic metal additives such as Hg and Pb.[14] Finally, the rate of H_2O_2 production is typically limited by diffusion of O_2 to the electrode, making it hard to access high production rates.[14,18,19] We acknowledge that peroxide solutions typically include stabilizers and one could, in principle, obviate the need for downstream separation by using a benign electrolyte that also served as the stabilizer. However, fulfilling these multiple requirements with a high-conductivity electrolyte remains challenging.

Anthraquinones themselves have been used in various electrochemical systems to produce H_2O_2, including with catalysts immobilized on electrodes,[23–25] in emulsion-type systems in conjunction with an alkaline aqueous phase,[26,27] and in aqueous solution under photoelectrochemical conditions.[28] However, to the best of our knowledge there are no examples of electrolyte-free H_2O_2 production using homogeneous electrochemical mediation.

We envisioned that all of the above challenges could be overcome simultaneously by integrating anthraquinone-mediated H_2O_2 generation with phase-transfer catalysis. In particular, we postulated that the following three-step sequence could allow for rapid, continuous H_2O_2 production and separation without the use of precious metal catalysts (Figure 1): the electrochemical reduction of a quinone to a hydroquinone in aqueous electrolyte; phase transfer of the hydroquinone into an immiscible solvent phase; and reaction of the hydroquinone with an oxygenated pure water stream to generate H_2O_2 and regenerate the original quinone for recycling to the electrochemical cell.

In this process, the quinone serves as both an electrochemical redox mediator and a phase-transfer agent for shuttling electron/proton equivalents between the electrolyte medium and pure water streams. As a result, this process substitutes the high energy and membrane costs of distillation or reverse osmosis with low-cost, low-energy, extraction-based separation steps.[29] While molecular redox mediation has

Please cite this article in press as: Murray et al., Electrosynthesis of Hydrogen Peroxide by Phase-Transfer Catalysis, Joule (2019), https://doi.org/10.1016/j.joule.2019.09.019

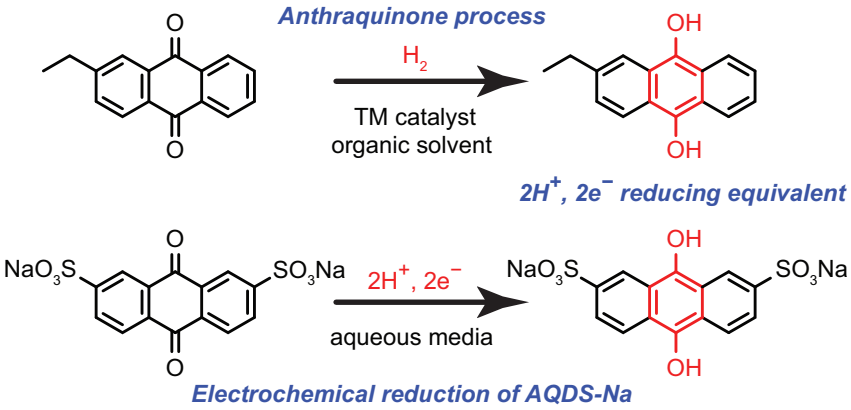

Figure 2. Anthraquinone Process (Top) and Electrochemical Reduction of $AQDS^{2-}$ to $AQDSH_2^{2-}$ (Bottom)

been applied to a variety of electrochemical transformations including water splitting[30–33] and oxygen reduction in fuel cells,[34,35] to best of our knowledge, it has never been applied in combination with phase-transfer catalysis to enable *in situ* product generation and separation.

Herein, we establish the feasibility of redox-mediated phase-transfer (RMPT) electrocatalysis and demonstrate that the approach enables continuous H_2O_2 electrosynthesis from H_2O and O_2 with simultaneous separation into an electrolyte-free aqueous product stream. We assemble an all-Earth-abundant proof-of-concept device that displays superior selectivity and H_2O_2 flux relative to reported direct electrosynthetic methods.

Electrochemistry of the Electron-Proton Transfer Mediator

The success of the proposed electrochemical phase-transfer scheme requires a molecular redox mediator with the following properties: (1) high solubility in water and an immiscible organic medium; (2) tunable phase-transfer properties; (3) reversible two-electron, two-proton redox chemistry; and (4) high activity for the selective conversion of O_2 to H_2O_2. Given the known activity and selectivity of dihydroanthraquinones used in industrial peroxide synthesis,[5] we adapted this core motif to the requirements of electrochemical RMPT H_2O_2 synthesis. To fulfill the requirement of selective transfer of quinone from the aqueous to an immiscible organic phase and vice versa, we sought an anionic anthroquinone derivative that could pair with hydrophilic and lipophilic cations in each respective phase. Specifically, we selected a dianionic anthraquinone with sulfonyl groups, 2,7-disulfonyl anthraquinone ($AQDS^{2-}$; Figure 2).[36]

The electrochemistry of $AQDS^{2-}$ is ideal for mediating peroxide synthesis, and our data establish that $AQDS^{2-}$ indeed undergoes selective two-electron, two-proton electroreduction to generate dihydroanthraquinone disulfonate ($AQDSH_2^{2-}$; Figure 2). In aqueous 0.1 M $HClO_4$, 20 mM $AQDS^{2-}$ displays a reversible redox wave at $E_{1/2}$ = 0.13 V versus the reversible hydrogen electrode (RHE) on glassy carbon electrodes (Figure 3A). This potential corresponds to a modest 0.55 V overpotential relative to the thermodynamic value for the O_2/H_2O_2 couple, providing ample driving force for the two-electron reduction of O_2 to H_2O_2. We observe a peak-to-peak separation of 90 mV, indicative of electrochemical quasireversibility, possibly due to quinone partial dimerization as previously reported.[37] Indeed, at higher concentrations still, it is likely that anthraquinones decompose in a bimolecular

Please cite this article in press as: Murray et al., Electrosynthesis of Hydrogen Peroxide by Phase-Transfer Catalysis, Joule (2019), https://doi.org/10.1016/j.joule.2019.09.019

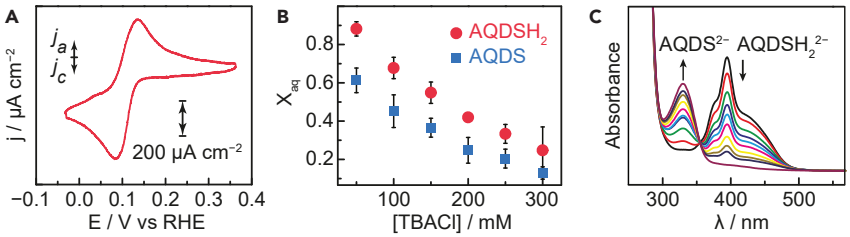

Figure 3. Phase Transfer and Redox Cycling of AQDS and AQDSH$_2$

(A) Cyclic voltammogram of 5 mM anthraquinone 2,7-disulfonic acid disodium salt ($AQDSNa_2$) in 0.1 M $HClO_4$.

(B) Water/1-hexanol partition coefficient, X_{aq}, for $AQDS^{2-}$ (blue squares) and $AQDSH_2^{2-}$ (red circles) in 0.1 M $HClO_4$ versus TBACl concentration in the 1-hexanol phase. Error bars show a standard deviation of the mean from the average of three runs.

(C) UV-vis time course over 25 min of the air oxidation of $AQDSH_2(TBA)_2$ in 1-hexanol.

fashion.[38] Nonetheless, the ratio of peak integrations, q_c/q_a, is 1.00, pointing to the chemical reversibility of this two-electron, two-proton process. In line with literature reports,[36] preparative electrolysis at 0.0 V versus RHE leads to clean conversion of the quinone to $AQDSH_2^{2-}$ as judged by UV visible (UV-vis) spectroscopy (Figure S1).[39] Since the carbon electrode does not catalyze hydrogen evolution or other reduction reactions at 0.0 V, we observe a high faradic efficiency, >95%, for the electrochemical conversion of $AQDS^{2-}$ to $AQDSH_2^{2-}$. Together, these observations establish that $AQDS^{2-}$ undergoes selective, high-yield, electrochemical reduction in acidic aqueous electrolytes.

Phase Transfer of the Mediator

Subsequently, we investigated the phase transfer of $AQDS^{2-}/AQDSH_2^{2-}$ from the aqueous $HClO_4$ electrolyte into an organic phase (Figure 4). We chose 1-hexanol as the organic phase for our application because of its low cost, low toxicity, and low miscibility with water as determined by ^1H NMR spectroscopy (Figure S2). Indeed, the current pharmaceutical industry best practice considers 1-hexanol a sustainable solvent for large-scale industrial use.[40] By controlling the cation composition of the aqueous and organic phases, we are able to systematically tune the phase-transfer equilibrium constant for both the oxidized and reduced forms of the mediator. For a 0.1 M $HClO_4$ aqueous phase in contact with 0.1 M tetrabutylammonium chloride (TBACl) in 1-hexanol, we observe a phase-transfer partition coefficient, X_{aq}, of 0.44 and 0.66 for $AQDS^{2-}$ and $AQDSH_2^{2-}$, respectively. The similar partition coefficients for the reduced and oxidized mediator suggest that the protonation/redox state of the quinone core does not dramatically alter the thermodynamics of phase transfer. Indeed, for this solvent mixture, we posit that the dominant driving force for phase transfer is the transfer of Cl^- ions from the organic phase to the aqueous phase. In line with this postulate, increasing the concentration of TBACl from 50 to 300 mM leads to a roughly linear decrease in X_{aq} from 0.61/0.84 to 0.16/0.22, respectively (Figure 3B). Additionally, over the entire range of TBACl electrolyte strengths, we observe a similar ratio of phase-transfer coefficients for $AQDS^{2-}$ and $AQDSH_2^{2-}$ of ~2:3. These partition coefficients are strongly dependent on the hydrogen-bonding properties of the organic phase—when 1-hexanol is substituted with dichloromethane, we observe partition coefficients, X_{aq}, of 0.64 and 0.95 for $AQDS^{2-}$ and $AQDSH_2^{2-}$, respectively, in the presence of 0.1 M TBACl (Figure S3). This suggests that a hydrogen-bonding organic solvent is required to facilitate the efficient transfer of $AQDSH_2^{2-}$ into the organic phase. These studies highlight the interplay between mediator charge, solvent, and ionic strength, all of which can be readily tuned to optimize the phase-transfer equilibrium. Together,

Please cite this article in press as: Murray et al., Electrosynthesis of Hydrogen Peroxide by Phase-Transfer Catalysis, Joule (2019), https://doi.org/10.1016/j.joule.2019.09.019

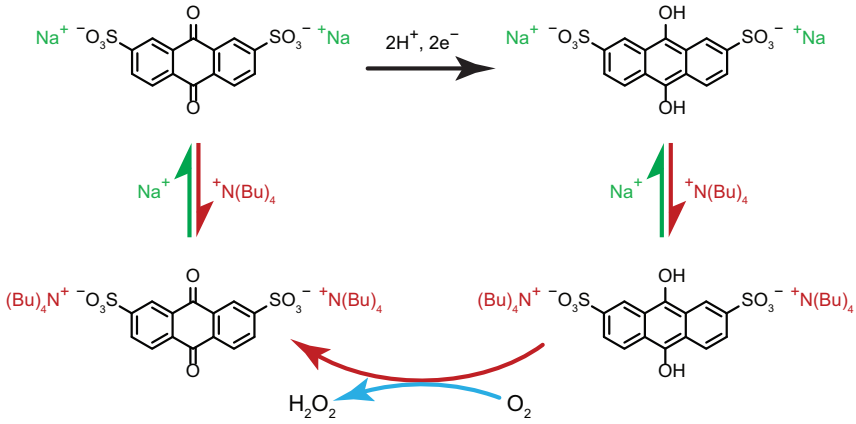

Figure 4. Phase Transfer Cycle for AQDS-Mediated H_2O_2 Production

Schematic depicting the electrochemical reduction of $AQDSNa_2$ to $AQDSH_2Na_2$ (top arrow), phase-transfer equilibration between $AQDSNa_2$ and $AQDS(TBA)_2$ (left), phase-transfer equilibration between $AQDSH_2(TBA)_2$ and $AQDSH_2Na_2$ (right), and mediated O_2 reduction to H_2O_2 (bottom arrows).

the data establish that both $AQDS^{2-}$ and $AQDSH_2^{2-}$ are able to reversibly transfer between $HClO_4$/water and TBACl/1-hexanol phases to facilitate RMPT H_2O_2 synthesis.

Synthesis of H_2O_2

Our data establish that the reduced anthraquinone, $AQDSH_2^{2-}$, promotes H_2O_2 production at the water/1-hexanol boundary, separating this reaction from the site of quinone reduction at the aqueous electrode. $AQDSH_2^{2-}$ rapidly converts O_2 to H_2O_2 in both the organic and aqueous phases. Following exposure of a 20 μM solution of $AQDSH_2(TBA)_2$ in 1-hexanol to air, we observe an isosbestic point at 355 nm in the UV-vis spectra, which is indicative of clean conversion of $AQDSH_2^{2-}$ to $AQDS^{2-}$ (Figure 3C). In the organic phase alone, this reaction is concluded in ~25 min, but its rate can be substantially accelerated by shaking with water, which leads to complete conversion in less than 15 s. Analysis of the water layer indicates the quantitative generation of one equivalent of H_2O_2 per $AQDSH_2^{2-}$ mediator. Importantly, we also observe complete retention of the $AQDS^{2-}$ in the 1-hexanol phase, with no transfer of reduced or oxidized quinone species to electrolyte-free water (Figure S4), as well as clean regeneration of $AQDS^{2-}$ upon H_2O_2 generation, with no detectable mediator degradation (Figure S5). We attribute this to a low concentration of phase-transfer-promoting ions in the aqueous phase and highlight the importance of this finding: indeed, phase-transfer electrosynthesis of H_2O_2 results in a product stream that consists only of peroxide and water, overcoming a key limitation of direct electrochemical H_2O_2 synthesis. While the complete mechanistic picture for H_2O_2 generation by $AQDSH_2^{2-}$ remains uncertain in this system, our data provide basic insight. The apparent rate acceleration in the presence of water suggests that proton transfer is key to the overall reaction. It is therefore possible that H_2O_2 forms via an endoperoxide-bridged species in analogy to the prevailing mechanistic model for H_2O_2 production in the anthraquinone process.[41,42] If this is the case, however, the intermediate appears to be in minor equilibrium, as indicated by our observation of an isosbestic point in the UV-vis data. Irrespective of the specific mechanism, the data establish that $AQDSH_2^{2-}$ rapidly generates aqueous H_2O_2 while regenerating $AQDS^{2-}$ in the organic phase for continuous recycling.

Please cite this article in press as: Murray et al., Electrosynthesis of Hydrogen Peroxide by Phase-Transfer Catalysis, Joule (2019), https://doi.org/10.1016/j.joule.2019.09.019

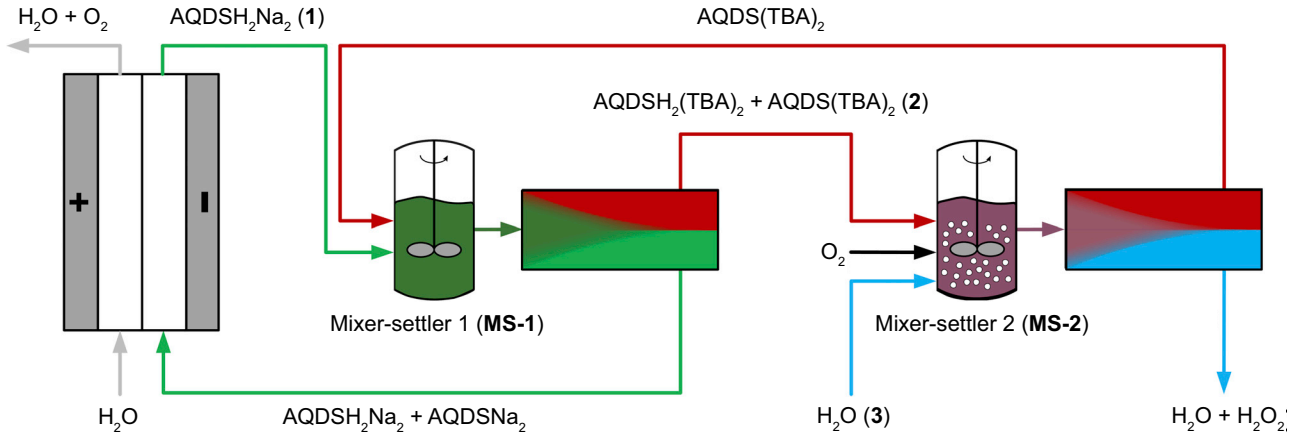

Figure 5. Detailed Scheme for the Proof-of-Concept H_2O_2 Synthesis/Separation Device

The scheme depicts the electrochemical cell (left), mixer-settler 1, **MS-1** (middle), and mixer-settler 2, **MS-2** (right). See Figure S6 for additional details.

Proof-of-Concept Process for Continuous H_2O_2 Synthesis

Taking advantage of the combined electrochemical, catalytic, and phase-transfer properties of $AQDS^{2-}$/$AQDSH_2^{2-}$, we designed a proof-of-concept process for continuous H_2O_2 generation (Figure 5). In this process, an acidic aqueous solution of $AQDS^{2-}$ is pumped past a carbon cathode to generate $AQDSH_2^{2-}$. This cathodic half-reaction is paired with anodic water oxidation to O_2, thereby enabling the complete conversion of water to O_2 and H_2O_2. With the goal of achieving an all-Earth-abundant device, we employed a commercially available Ni foam as the anode material and oxygen-evolving catalyst.[43] Nickel oxide performs oxygen evolution most effectively and durably in an alkaline environment, while $AQDS^{2-}$ reduction is most efficient in an acidic environment. To satisfy the disparate pH requirements of the anode and cathode reactions, we employed a bipolar membrane to effectively separate the cathodic and anodic environments within our cell. Upon polarization, the electric field across this bipolar membrane promotes the dissociation of water into H^+ and OH^-, thereby generating a pH gradient across the cell that serves to replenish the protons consumed during $AQDS^{2-}$ reduction and the OH^- ions consumed during oxygen evolution.[44] We note that this bipolar membrane also serves to inhibit the crossover of the redox mediator between anode and cathode compartments, ensuring a sustained pool of the mediator available for continuous H_2O_2 generation.

Following the electrochemical reduction of $AQDS^{2-}$, the resulting aqueous $AQDSH_2^{2-}$ stream is contacted with the 1-hexanol phase. The two phases are vigorously mixed and subsequently separated using a "mixer-settler" (Figures S7 and S8) apparatus commonly employed for phase-transfer separations.[45] This first mixer-settler (**MS-1**) partitions the reduced and oxidized quinones between the two phases. The aqueous stream is fed back into the electrochemical cell, whereas the organic stream, now containing $AQDSH_2^{2-}$, is contacted with O_2 and water in a second mixer-settler (Figure S8). In this second step, O_2 is rapidly converted to H_2O_2, regenerating the $AQDS^{2-}$ mediator. As described above, the $AQDS^{2-}$ remains in the 1-hexanol phase and is recycled to the first mixer-settler, while pure H_2O_2 partitions preferentially into the water phase for isolation. Importantly, this continuous process generates H_2O_2 remote from the membrane and the electrolytic cell. In addition to producing electrolyte-free H_2O_2, this process eliminates the possibility of oxidative damage to the polymer membrane and catalytic disproportionation of H_2O_2 to water and O_2 by the cathode material. Thus, through the simple

Please cite this article in press as: Murray et al., Electrosynthesis of Hydrogen Peroxide by Phase-Transfer Catalysis, Joule (2019), https://doi.org/10.1016/j.joule.2019.09.019

combination of a pump and two mixer-settlers, this phase-transfer system achieves the electrosynthesis of pure aqueous H_2O_2, with the quinone mediator acting as a proton- and electron-transfer agent.

Efficient H_2O_2 production in this mediated system relies on efficient gas transport into the reacting phases. Indeed, if O_2-saturated water is contacted with the organic phase in the second mixer-settler (**MS-2**), the maximum single pass H_2O_2 concentration is limited to the 1 mM O_2 solubility in water. However, we found that this limit could be easily exceeded by continuously bubbling O_2 into the mixing zone of **MS-2**. In this configuration, shrinking gas bubbles provide a constant supply of dissolved oxygen in the aqueous phase to match the rapid rate of H_2O_2 production at the water/hexanol interface.[36] While the studies reported here were conducted with a 1.0 atm O_2 feed, we stress that $AQDSH_2^{2-}$ also reacts rapidly with air (see above and Figure 3C). Thus, the process can be readily adapted to an air stream by matching the flux of mediator and gas streams to the lower atmospheric O_2 partial pressure. Irrespective of the O_2 source, matching the fluxes of O_2 and $AQDSH_2^{2-}$ mediator is critical for preventing O_2 permeation throughout the rest of the system.

Our proof-of-concept device is effective for continuous, long-term H_2O_2 production. We observe stable current densities, *j*, between 8 and 10 mA cm^{-2} (relative to the geometric area of the electrochemical cell, see Figure S9) over the course of 7 h of continuous operation at an applied cell voltage of 2.25 V. This cell voltage includes significant contributions from parasitic resistive losses in the 26 cm^2 prototype cell we employed. From current-voltage data (Figure S10), we estimate a lower bound of the effective cell resistance of ~4.5 Ω, leading to an estimated iR-free (corrected for uncompensated resistance) cell voltage of ~1.4 V. We envision that further cell engineering and/or increased aqueous electrolyte strength should be able to minimize these resistive losses and reduce the operating voltage.[46] The H_2O_2 concentration in the final output water stream was periodically quantified by iodometric titration, revealing that the H_2O_2 production rate (Figure 6A, blue) corresponds to near quantitative faradic efficiency for H_2O_2 production (Figure 6A, red). This efficiency decreases slightly to ~80% over many hours of operation, an effect which we attribute to parasitic H_2 evolution at the cathode and/or adventitious disproportionation of the produced H_2O_2. These challenges can be addressed by optimizing the flow field in the electrochemical cell and minimizing trace metal impurities on the side walls of the mixer-settlers (particularly in the gas-mixing zone of MS-2 where local H_2O_2 concentrations are high), respectively. Notwithstanding, the partial current density contributing to mediated H_2O_2 production in this system remains in excess of 8 mA cm^{-2} over long-term operation. This value greatly exceeds the diffusion-limited rate of direct O_2 reduction to H_2O_2 of < 3 mA cm^{-2} on an electrode rotated at 2000 rpm, highlighting the value of this approach for high flux H_2O_2 production.[47] Additionally, our H_2O_2 production rate, v_d, (3 μmol min^{-1} cm^{-2}) rivals optimized values for polymer acidic electrolyte devices that operate at a significantly higher temperature and oxygen flux with lower faradic efficiencies (30%).[18] While a recently reported neutralization cell device achieves high faradic efficiencies at high production rates,[20] crossover of H_2O_2 to the anode degrades faradic efficiencies at high H_2O_2 concentration; the RMPT approach directly addresses this problem.

Importantly, the current density and flow rate ratios can be independently controlled to set the desired concentration of peroxide in the aqueous output stream. Varying the current density of mediator regeneration over a range of 2 to 10 mA cm^{-2} leads to a roughly linear increase in H_2O_2 production rate (Figure 6B, blue), consistent with the high faradic efficiency of the process (Figure 6B, red). Likewise, varying the flow rate of the aqueous product stream, **3**, relative to the mediator recycle loop, **2**,

Please cite this article in press as: Murray et al., Electrosynthesis of Hydrogen Peroxide by Phase-Transfer Catalysis, Joule (2019), https://doi.org/10.1016/j.joule.2019.09.019

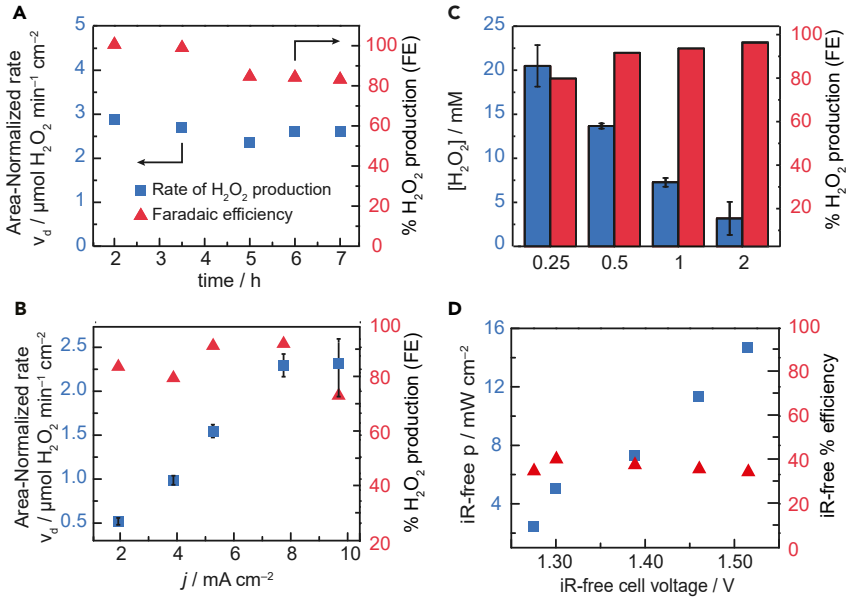

Figure 6. Performance of Flow Electrolyzer for Mediated H_2O_2 Electrosynthesis

(A) Area-normalized rate of H_2O_2 production, v_d (left axis, blue squares), and faradic efficiency (right axis, red triangles) versus time.

(B) H_2O_2 production rate (left axis, blue squares) and faradic efficiency (right axis, red triangles) versus the applied current density, *j*.

(C) Steady-state H_2O_2 concentration in the product stream (left axis, blue bars) and faradic efficiency (right axis, red bars) versus the ratio of flow rates of streams **2** and **3** (see Figure 5).

(D) Power density consumed by the device (left axis, blue squares), and iR-free % efficiency for H_2O_2 production (right axis, red triangles), as a function of the iR-free cell voltage. Error bars show a standard deviation of the mean from the average of three runs.

permits *selection* of the concentration of H_2O_2 in the product stream. Indeed, by reducing the flow ratio, we obtain a higher H_2O_2 concentration and can access a more dilute H_2O_2 stream by increasing the flow ratio (Figure 6C, blue), all while maintaining a high faradic efficiency (Figure 6C, red). Over all of these conditions, we observe a continuous production rate of H_2O_2 of 2–3 µmol min^{-1} cm^{-2} for many hours and have been able to access H_2O_2 concentrations of 33 mM (Figure S11).

The device consumes a modest amount of power, <10 mW cm^{-2}, suitable for distributed or remote operation. Furthermore, since *in situ* product separation proceeds passively via phase transfer, the system only draws power to drive the electrochemical cell and pump the non-viscous solutions. Thus, the overall energy efficiency of the process, neglecting pumping costs, can be calculated based on the cell voltage. Excluding resistivity losses, the process displays an energetic efficiency of ~40% across a wide range of current densities (Figures 6D and S12). Together, these observations highlight the inherent advantages of mediated electrolysis, particularly for the production of H_2O_2.

Conclusions and Outlook

In summary, we have employed a RMPT approach to produce and isolate aqueous H_2O_2 from the electrolysis of H_2O and O_2. Generally, the development of electrochemical processes often ignores the energy and capital costs associated with the separation and purification of the value-added product. Particularly for liquid products, these separation costs cannot be ignored. By employing a redox mediator

Please cite this article in press as: Murray et al., Electrosynthesis of Hydrogen Peroxide by Phase-Transfer Catalysis, Joule (2019), https://doi.org/10.1016/j.joule.2019.09.019

that can be easily phase separated, we showcase the power of the RMPT approach to facilitate simultaneous production and separation of a liquid product within an integrated electrochemical/phase-transfer process for the first time. This concept has broad implications because the functionality of the mediator can also be purposefully designed to deliver redox equivalents to reaction/separation environments that would be incompatible with their generation. Indeed, there is growing evidence that the uncontrolled proton donor environment of aqueous electrolytes, combined with the nucleophilicity of hydroxide, compromises the efficiency and selectivity of more complex reactions including CO_2 reduction,[48,49] N_2 reduction,[50,51] and NH_3 oxidation.[52] Additionally, in the context of organic electrosynthesis, many substrates are simply not soluble in aqueous media. In all of these electrochemical processes, our RMPT approach could be used to drive difficult redox transformations in non-aqueous environments that are incompatible with electrochemistry but are ideal for maximizing substrate solubility and enhancing reaction selectivity and efficiency. Thus, by decoupling the conditions of electrochemistry from the conditions ideal for substrate turnover and separation, the RMPT approach established here enables a vast expansion of the utility of electrochemical processes.

EXPERIMENTAL PROCEDURES

Batch Electrochemical Characterization

Cyclic voltammetry and chronoamperometry were recorded using a Biologic VSP 16-channel potentiostat, a glassy carbon working electrode, platinum counter electrode, and a Ag/AgCl reference electrode (see Supplemental Experimental Procedures for further details)

Determination of Partition Coefficients

Two phases (20 mM $AQDSNa_2$ in 0.1 M $HClO_4$ and TBACl in 1-hexanol) were shaken in a vial and allowed to separate for 5 min. Subsequently, the amount of quinone remaining in the aqueous layer was measured by UV-vis spectroscopy.[14] The same procedure was used for $AQDSH_2Na_2$, which was prepared by bulk electrolysis of $AQDSNa_2$.

Quinone Autooxidation

20 mM $AQDSNa_2$ in 0.1 M $HClO_4$ aqueous electrolyte was fully reduced in a flow cell, under N_2. The reduced quinone $AQDSH_2^{2-}$ was then extracted into 0.1 M TBACl in 1-hexanol under N_2. The organic hexanol phase was transferred into a cuvette that was purged with N_2, and the first spectrum of the fully reduced quinone was recorded. The cap of the cuvette was then removed to allow oxygen dissolution and diffusion into 1-hexanol for the slow oxidation of the reduced quinone. Spectra were recorded every 2 min. The full oxidation was achieved within 25 min.

Flow Electrochemical Cell Fabrication

The electrochemical cell was fabricated using 3″ × 3″, 1/8″ thick, 316 stainless steel sheet current collectors. Silicone rubber sheets (50A Durometer) containing 2″ × 2″ cavities served as gaskets. Four overlapping 2″ × 2″ graphite felt pieces were used as the cathode, and three overlapping 2″ × 2″ nickel foam sheets were used as the anode. Polyproylene inlet and outlet fittings were inserted into the sides of the silicone sheets to allow for anolyte and catholyte circulation flows. The two half-cells were separated by a 3″ × 3″ bipolar membrane. The exposed electrode area of the cell was 2″ × 2″ (25.8 cm^2).

Please cite this article in press as: Murray et al., Electrosynthesis of Hydrogen Peroxide by Phase-Transfer Catalysis, Joule (2019), https://doi.org/10.1016/j.joule.2019.09.019

Mixer-Settler Fabrication

MS-1 was machined from polypropylene. The mixing zone was a cylindrical cup, with liquid inlets on both sides at the bottom, and was separated from the settling zone by an emulsion overflow and a baffle. The settling zone had three coalescence plates, to enhance phase separation, and a light phase weir to allow for level fluctuations. The volumes of the mixing and settling zones were ~100 mL each, resulting in a total holdup volume of ~200 mL. **MS-2** was custom fabricated from glass by James Glass Inc. and was of similar intrinsic design with the additional ability to bubble gas streams into the mixing zone. See Supplemental Experminetal Procedures for full details.

Device Operation

Surge tanks in the flow system (Figure S6) were charged with the appropriate solutions (Table S2). The first mixer-settler, in **MS-1**, was primed by syringe addition of 100 mL each of 20 mM $AQDS^{2-}$/0.1 M $HClO_4$ and 20 mM $AQDS^{2-}$/0.1 M TBACl/1-hexanol. The second mixer-settler, **MS-2**, was primed with 110 mL each of water, stabilized with 1 mM Na_2EDTA and 3 mM citric acid, and 0.1 M TBACl/1-hexanol. The pumps (Cole-Parmer, Masterflex) were run at 10 mL min^{-1} for 20 min to allow the system to reach equilibrium before electrochemistry or O_2 sparging was commenced. Tanks T-2, T-3, and T-4 (Figure S6) were constantly bubbled with nitrogen to prevent oxygen from **MS-2**, carried by the organic phase, from entering the electrochemical cell during the operation of the system. The flow system was operated at ambient temperature, 20°C–22°C. The system was operated at constant potential or current, depending on the experiment.

H_2O_2 Quantification

H_2O_2 was quantified by iodometric titration according to a standard procedure.[11] An aliquot of KI in H_2SO_4 was added to the test sample to generate I_2, which was titrated by quenching with a standard solution of 0.1 M $Na_2S_2O_3$ until the color disappeared. Peroxide titrations were periodically cross-checked using peroxidase-based semi-quantitative test strips (Millipore MQuant, 0–100 ppm/100–1,000 ppm, LaMotte InstaTest 0–90 ppm, 1 mM = 34 ppm).

SUPPLEMENTAL INFORMATION

Supplemental Information can be found online at https://doi.org/10.1016/j.joule.2019.09.019.

ACKNOWLEDGMENTS

This research was primarily supported as part of the Center for Molecular Electrocatalysis, an Energy Frontier Research Center funded by the U.S. Department of Energy (DOE), Office of Science, Basic Energy Sciences (BES). Partial support for device fabrication was provided by the Tata Institute for Design at MIT. M.S. acknowledges fellowship support from the Swiss National Science Foundation. A.T.M. acknowledges the Camille and Henry Dreyfus Postdoctoral Program in Environmental Chemistry for fellowship support. Y.S. acknowledges the Sloan Foundation, Research Corporation for Science Advancement (Cottrell Scholar), and the Canadian Institute for Advanced Research (CIFAR Azrieli Global Scholar).

AUTHOR CONTRIBUTIONS

A.T.M. and S.V. are co-first authors. Y.S., T.A.H., A.M., S.V., and M.S. conceived and designed the experimental investigations. A.T.M. and S.V. performed experiments. Y.S., T.A.H., A.T.M., S.V., and M.S. analyzed the data and wrote the paper.

DECLARATION OF INTERESTS

Y.S., T.A.H., A.T.M., and S.V. are inventors on provisional patent application 62/718,745 filed by the Massachusetts Institute of Technology that covers the electrochemical peroxide production method reported in this work.

Received: August 6, 2019
Revised: September 18, 2019
Accepted: September 26, 2019
Published: October 24, 2019

REFERENCES

1. McDonnell, G. (2014). The use of hydrogen peroxide for disinfection and sterilization applications. In PATAI's Chemistry of Functional Groups (American Cancer Society), pp. 1–34.
2. Oller, I., Malato, S., and Sánchez-Pérez, J.A. (2011). Combination of advanced oxidation processes and biological treatments for wastewater decontamination—a review. Sci. Total Environ *409*, 4141–4166.
3. Butkovskyi, A., Bruning, H., Kools, S.A.E., Rijnaarts, H.H.M., and Van Wezel, A.P. (2017). Organic pollutants in shale gas flowback and produced waters: identification, potential ecological impact, and implications for treatment strategies. Environ. Sci. Technol *51*, 4740–4754.
4. Bartram, J., and Cairncross, S. (2010). Hygiene, sanitation, and water: forgotten foundations of health. PLoS Med *7*, e1000367.
5. Riedl, H.-J., and Pfleiderer, G. (1939). Production of hydrogen peroxide. US Patent US 2,158,525, 1939.
6. Campos-Martin, J.M., Blanco-Brieva, G., and Fierro, J.L.G. (2006). Hydrogen peroxide synthesis: an outlook beyond the anthraquinone process. Angew. Chem. Int. Ed. Engl. *45*, 6962–6984.
7. Merchant research and Consulting Ltd., hydrogen peroxide (HP): 2015 world market outlook. (2015). (Merchant Research and Consulting Ltd.).
8. McIntyre, J.A., and Phillips, R.F. (1984). Method for electrolytic production of alkaline peroxide solutions. US Patent US 4,431,494 A.
9. Liu, Y., Quan, X., Fan, X., Wang, H., and Chen, S. (2015). High-yield electrosynthesis of hydrogen peroxide from oxygen reduction by hierarchically porous carbon. Angew. Chem. Int. Ed. Engl. *54*, 6837–6841.
10. Thostenson, J.O., Ngaboyamahina, E., Sellgren, K.L., Hawkins, B.T., Piascik, J.R., Klem, E.J.D., Parker, C.B., Deshusses, M.A., Stoner, B.R., and Glass, J.T. (2017). Enhanced H_2O_2 production at reductive potentials from oxidized boron-doped ultrananocrystalline diamond electrodes. ACS Appl. Mater. Interfaces *9*, 16610–16619.
11. Chen, Z., Chen, S., Siahrostami, S., Chakthranont, P., Hahn, C., Nordlund, D., Dimosthenis, S., Nørskov, J.K., Bao, Z., and Jaramillo, T.F. (2017). Development of a reactor with carbon catalysts for modular-scale, low-cost electrochemical generation of H_2O_2. React. Chem. Eng *2*, 239–245.
12. Iglesias, D., Giuliani, A., Melchionna, M., Marchesan, S., Criado, A., Nasi, L., Bevilacqua, M., Tavagnacco, C., Vizza, F., Prato, M., et al. (2018). N-doped graphitized carbon nanohorns as a forefront electrocatalyst in highly selective O_2 reduction to H_2O_2. Chem *4*, 106–123.
13. Lu, Z., Chen, G., Siahrostami, S., Chen, Z., Liu, K., Xie, J., Liao, L., Wu, T., Lin, D., Liu, Y., et al. (2018). High-efficiency oxygen reduction to hydrogen peroxide catalysed by oxidized carbon materials. Nat. Catal. *1*, 156–162.
14. Siahrostami, S., Verdaguer-Casadevall, A., Karamad, M., Deiana, D., Malacrida, P., Wickman, B., Escudero-Escribano, M., Paoli, E.A., Frydendal, R., Hansen, T.W., et al. (2013). Enabling direct H_2O_2 production through rational electrocatalyst design. Nat. Mater. *12*, 1137–1143.
15. Jirkovský, J.S., Panas, I., Ahlberg, E., Halasa, M., Romani, S., and Schiffrin, D.J. (2011). Single atom hot-spots at Au–Pd nanoalloys for electrocatalytic H_2O_2 production. J. Am. Chem. Soc. *133*, 19432–19441.
16. Verdaguer-Casadevall, A., Deiana, D., Karamad, M., Siahrostami, S., Malacrida, P., Hansen, T.W., Rossmeisl, J., Chorkendorff, I., and Stephens, I.E.L. (2014). Trends in the electrochemical synthesis of H_2O_2: enhancing activity and selectivity by electrocatalytic site engineering. Nano Lett. *14*, 1603–1608.
17. Pizzutilo, E., Freakley, S.J., Cherevko, S., Venkatesan, S., Hutchings, G.J., Liebscher, C.H., Dehm, G., and Mayrhofer, K.J.J. (2017). Gold–palladium bimetallic catalyst stability: consequences for hydrogen peroxide selectivity. ACS Catal *7*, 5699–5705.
18. Li, W., Bonakdarpour, A., Gyenge, E., and Wilkinson, D.P. (2013). Drinking water purification by electrosynthesis of hydrogen peroxide in a power-producing PEM fuel cell. ChemSusChem *6*, 2137–2143.
19. Yang, S., Verdaguer-Casadevall, A., Arnarson, L., Silvioli, L., Čolić, V., Frydendal, R., Rossmeisl, J., Chorkendorff, I., and Stephens, I.E.L. (2018). Toward the decentralized electrochemical production of H_2O_2: a focus on the catalysis. ACS Catal. *8*, 4064–4081.
20. Xia, C., Xia, Y., Zhu, P., Fan, L., and Wang, H. (2019). Direct electrosynthesis of pure aqueous H_2O_2 solutions up to 20% by weight using a solid electrolyte. Science *366*, 226–231.
21. Otsuka, K., and Yamanaka, I. (1990). One step synthesis of hydrogen peroxide through fuel cell reaction. Electrochim. Acta *35*, 319–322.
22. Yamanaka, I., and Murayama, T. (2008). Neutral H_2O_2 synthesis by electrolysis of water and O_2. Angew. Chem. Int. Ed. Engl. *47*, 1900–1902.
23. Vaik, K., Mäeorg, U., Maschion, F.C., Maia, G., Schiffrin, D.J., and Tammeveski, K. (2005). Electrocatalytic oxygen reduction on glassy carbon grafted with anthraquinone by anodic oxidation of a carboxylate substituent. Electrochim. Acta *50*, 5126–5131.
24. Forti, J.C., Rocha, R.S., Lanza, M.R.V., and Bertazzoli, R. (2007). Electrochemical synthesis of hydrogen peroxide on oxygen-fed graphite/PTFE electrodes modified by 2-ethylanthraquinone. J. Electroanal. Chem. *601*, 63–67.
25. Valim, R.B., Reis, R.M., Castro, P.S., Lima, A.S., Rocha, R.S., Bertotti, M., and Lanza, M.R.V. (2013). Electrogeneration of hydrogen peroxide in gas diffusion electrodes modified with tert-butyl-anthraquinone on carbon black support. Carbon *61*, 236–244.
26. Huissoud, A., and Tissot, P. (1999). Electrochemical reduction of 2-ethyl-9,10-anthraquinone (EAQ) and mediated formation of hydrogen peroxide in a two-phase medium part I: Electrochemical behaviour of EAQ on a vitreous carbon rotating disc electrode (RDE) in the two-phase medium. J. Appl. Electrochem. *29*, 11–16.
27. Huissoud, A., and Tissot, P. (1999). Electrochemical reduction of 2-ethyl-9,10-anthraquinone (EAQ) and mediated formation of hydrogen peroxide in a two-phase medium part II: production of alkaline hydrogen peroxide by the intermediate electroreduction of EAQ in a flow-by porous electrode in two-phase liquid–liquid flow. J. Appl. Electrochem. *29*, 17–25.
28. Keita, B., and Nadjo, L. (1984). Electrochemistry and photoelectrochemistry of sodium 9,10-anthraquinone-2,6-disulfonate in aqueous media. J. Electroanal. Chem. Interfacial Electrochem. *163*, 171–188.
29. Fair, J.R., and Humphrey, J.L. (1984). Liquid-liquid extraction: possible alternative to distillation. Solvent Extr. Ion Exch. *2*, 323–352.
30. Symes, M.D., and Cronin, L. (2013). Decoupling hydrogen and oxygen evolution during electrolytic water splitting using an electron-coupled-proton buffer. Nat. Chem. *5*, 403–409.

31. Rausch, B., Symes, M.D., and Cronin, L. (2013). A bio-inspired, small molecule electron-coupled-proton buffer for decoupling the half-reactions of electrolytic water splitting. J. Am. Chem. Soc. *135*, 13656–13659.

32. Rausch, B., Symes, M.D., Chisholm, G., and Cronin, L. (2014). Decoupled catalytic hydrogen evolution from a molecular metal oxide redox mediator in water splitting. Science *345*, 1326–1330.

33. Kirkaldy, N., Chisholm, G., Chen, J.J., and Cronin, L. (2018). A practical, organic-mediated, hybrid electrolyser that decouples hydrogen production at high current densities. Chem. Sci. *9*, 1621–1626.

34. Anson, C.W., and Stahl, S.S. (2017). Cooperative electrocatalytic O_2 reduction involving Co(salophen) with p-hydroquinone as an electron–proton transfer mediator. J. Am. Chem. Soc. *139*, 18472–18475.

35. Preger, Y., Gerken, J.B., Biswas, S., Anson, C.W., Johnson, M.R., Root, T.W., and Stahl, S.S. (2018). Quinone-mediated electrochemical O_2 reduction accessing high power density with an off-electrode Co-N/C catalyst. Joule *2*, 2722–2731.

36. Huskinson, B., Marshak, M.P., Suh, C., Er, S., Gerhardt, M.R., Galvin, C.J., Chen, X., Aspuru-Guzik, A., Gordon, R.G., and Aziz, M.J. (2014). A metal-free organic–inorganic aqueous flow battery. Nature *505*, 195–198.

37. Carney, T.J., Collins, S.J., Moore, J.S., and Brushett, F.R. (2017). Concentration-dependent dimerization of anthraquinone disulfonic acid and its impact on charge storage. Chem. Mater. *29*, 4801–4810.

38. Wermeckes, B., and Beck, F. (1994). Acid-catalyzed disproportionation of anthrahydroquinone to anthraquinone and anthrone. Denki kagaku *62*, 1202–1205.

39. Gamage, R.S.K.A., McQuillan, A.J., and Peake, B.M. (1991). Ultraviolet–visible and electron paramagnetic resonance spectroelectrochemical studies of the reduction products of some anthraquinone sulphonates in aqueous solutions. J. Chem. Soc. Faraday Trans. *87*, 3653–3660.

40. Alder, C.M., Hayler, J.D., Henderson, R.K., Redman, A.M., Shukla, L., Shuster, L.E., and Sneddon, H.F. (2016). Updating and further expanding GSK's solvent sustainability guide. Green Chem. *18*, 3879–3890.

41. Arpe, H.J., and Weissermel, K. (2003). Industrial Organic Chemistry, pp. 329–330.

42. Nishimi, T., Kamachi, T., Kato, K., Kato, T., and Yoshizawa, K. (2011). Mechanistic study on the production of hydrogen peroxide in the anthraquinone process. Eur. J. Org. Chem. *2011*, 4113–4120.

43. Trotochaud, L., Young, S.L., Ranney, J.K., and Boettcher, S.W. (2014). Nickel–iron oxyhydroxide oxygen-evolution electrocatalysts: the role of intentional and incidental iron incorporation. J. Am. Chem. Soc. *136*, 6744–6753.

44. Schreier, M., Héroguel, F., Steier, L., Ahmad, S., Luterbacher, J.S., Mayer, M.T., Luo, J., and Grätzel, M. (2017). Solar conversion of CO_2 to CO using Earth-abundant electrocatalysts prepared by atomic layer modification of CuO. Nat. Energy *2*, 17087.

45. Alter, H.W., Codding, J.W., and Jennings, A.S. (1954). Miniature mixer settler for continuous countercurrent solvent extraction. Anal. Chem. *26*, 1357–1361.

46. Ke, X., Prahl, J.M., Alexander, J.I.D., Wainright, J.S., Zawodzinski, T.A., and Savinell, R.F. (2018). Rechargeable redox flow batteries: flow fields, stacks and design considerations. Chem. Soc. Rev. *47*, 8721–8743.

47. Treimer, S., Tang, A., and Johnson, D.C. (2002). A consideration of the application of Koutecký-Levich plots in the diagnoses of charge-transfer mechanisms at rotated disk electrodes. Electroanalysis *14*, 165–171.

48. Zhang, B.A., Ozel, T., Elias, J.S., Costentin, C., and Nocera, D.G. (2019). Interplay of homogeneous reactions, mass transport, and kinetics in determining selectivity of the reduction of CO_2 on gold electrodes. ACS Cent. Sci. *5*, 1097–1105.

49. Zhang, B.A., Costentin, C., and Nocera, D.G. (2019). On the conversion efficiency of CO_2 electroreduction on gold. Joule *3*, 1565–1568.

50. Deng, J., Iñiguez, J.A., and Liu, C. (2018). Electrocatalytic nitrogen reduction at low temperature. Joule *2*, 846–856.

51. Andersen, S.Z., Čolić, V., Yang, S., Schwalbe, J.A., Nielander, A.C., McEnaney, J.M., Enemark-Rasmussen, K., Baker, J.G., Singh, A.R., Rohr, B.A., et al. (2019). A rigorous electrochemical ammonia synthesis protocol with quantitative isotope measurements. Nature *570*, 504–508.

52. Bunce, N.J., and Bejan, D. (2011). Mechanism of electrochemical oxidation of ammonia. Electrochim. Acta *56*, 8085–8093.